# ULTRASONIC DETERMINATION OF RECRYSTALLIZATION

Edward R. Generazio

National Aeronautics and Space Administration
Lewis Research Center
Cleveland, OH.

## INTRODUCTION

Metals are currently used in a wide variety of applications ranging from simple structural to complex heat engine components. Each use has a different set of engineering characteristics that must be met by the material being considered for use. One method to tailor material properties to meet engineering requirements is thermomechanical processing (TMP).[1,2] If TMP involves cold working, metals generally show a marked increase in strength, but this increase does not continue without limit as the microstructure becomes distorted and exhibits high internal stress. These residual stresses are generally detrimental to the end use applications.

It is shown here that the nondestructive measurement of ultrasonic attenuation can identify and characterize the state of the recrystallization. The interrelation between ultrasonic attenuation and recrystallization thermal kinetics yields a technique for determining onset, degree, and completion of recrystallization.

## THEORY

We are concerned here with the ultrasonic interaction with material microstructure and the thermal process of recrystallization. Two theories covering acoustic-microstructure[5-7] interaction and the thermal kinetics of recrystallization[8-10] need to be examined. It is assumed that the acoustic interaction with the microstructure is dominated by grain scattering[6] and/or dislocation damping.[7] Other acoustic-microstructural interactions leading to magnetoelastic and thermoelastic effects[5] are not expected to change substantially and/or concurrently with recrystallization.

The attenuation $a_g$ due to grain scattering is given by[6]

$$a_r = C_r D^3 F^4 \text{(Rayleigh)} \quad \text{and} \quad a_s = C_s D F^2 \text{ (Stochastic)} \tag{1}$$

where the C's are constants dependent on density, velocity, etc., D is the mean grain diameter, F is frequency. When the wavelength of sound is much greater than the mean grain diameter or scatterer size, we have

Rayleigh scattering with a fourth power frequency dependence. When the scatterer size is on the order of the sound wavelength we have stochastic scattering with a second power frequency dependence. Equation (1) should not be expected to apply to an arbitrary metal consisting of a size distribution of topologically complex grains. However, we may identify the frequency exponent as a key variable. That is, if grains are growing from small (Rayleigh) to large (stochastic) scatterers is is expected that the frequency exponent, over a fixed frequency range, should decrease with increasing grain size.

The attenuation due to dislocation damping $a_d$ is given by[7]

$$a_d = gCW(F,F_0) \tag{2}$$

where $g$ is the dislocation density, $C$ is a constant dependent on shear modulus, dislocation damping force, etc., and $W$ is a complicated function of the resonant frequency $F_0$. Equation (2) applies to materials containing a dilute noninteracting collection of dislocation lines oriented normal to the sound direction. Equation (2) does not apply to the intertwined network of dislocations observed in mechanically worked materials. Equation (2) does, however, imply that if dislocation damping is dominant attenuation mechanism then a decrease in dislocation density should result in a corresponding decrease in attenuation.

## THERMAL KINETICS

Mechanically working a metal produces a dense collection of germ nuclei within the material. These germ nuclei, when activated by an increase in temperature, transform (i.e., recrystallize) into small crystallites which subsequently grow into fully developed grains. The transformed volume is given by[8-10]

$$\frac{V_R}{V} = \sum_{i=1}^{M} \left\{ 1 - \exp\left[ -SG^3 N_0 t^3 \exp\left( -\frac{U}{RT_i} \right) \right] \right\} \tag{3}$$

where $V_R$ is the volume that has recrystallized and $V$ is the initial unrecrystallized volume, and

- $S$ shape factor
- $G$ grain growth rate
- $R$ gas constant
- $N_0$ initial number of germ nuclei per unit volume
- $U$ total energy required for a germ nuclei to become a growth nucleus (crystallite)
- $T_i$ absolute anneal temperature
- $t$ anneal time

Equation (3) is applicable to thermal annealing processes, where the time of each anneal is held constant and the anneal temperature $T_i$ is varied for a series of $M$ anneals.

Although $G$, $U$, $S$, and $N_0$ are known to vary with temperature,[1,3,4,8-10] the value of these parameters as a function of temperature is unknown. It will be assumed that they are constants and this should be considered when using the thermal kinetic results.

## Material Samples

The samples were produced from commercially available Nickel 200 rod that has been initially cold rolled 50 percent and annealed at 631±5 K for 15 min, then cold rolled an additional 50 percent. Four samples for ultrasonic evaluation were cut from the rolled material with both sides ground and polished through 1.0 μm diamond to a mirror finish. Thirty-two specimens for metallographic, x-ray, and transmission electron microscopic analysis were also cut from the rolled stock.

## Experiment

The 36 specimens (anneal batch) were initially simultaneously annealed as a group in air at 758 K for 1 hr and air cooled. Two metallography specimens were selected and permanently removed from the group for microstructural, x-ray, and transmission electron microscopic evaluation, and the four polished samples were remeasured for thickness and ultrasonic attenuation (30 to 65 MHz).[11] After ultrasonic investigation these four samples and the remaining 30 specimens were heat treated at a higher temperature. This process of specimen selection (permanent removal of two specimens) and ultrasonic evaluation of the four polished samples was repeated 16 times with the annealing temperature increased for each step and ranging from 758 to 1011 K (±5 K). The two specimens removed after each step were investigated using: (1) metallography to determine microstructural changes, (2) transmission electron microscopy to identify dislocation density variations, and (3) x-ray diffraction to determine crystalline disorder.

## Microstructure

Three mutually perpendicular faces of the annealed samples were polished, etched, and photographed using standard metallographic procedures.

Three millimeter diameter, 0.38 mm thick disks were electro-discharge machined (EDM) from the annealed specimens. After the disks were hand ground to a thickness of about 0.002 cm and further electropolished to a thickness of about 800 Å, they were examined by transmission electron microscopy (TEM). At least three TEM disks were examined for each annealing temperature.

# RESULTS

## Ultrasonic Attenuation

The ultrasonic attenuation as a function of frequency for each of the annealing temperatures is shown in Fig. 1 and the attenuation for fixed frequency is illustrated as a function of anneal temperature in Fig. 2. While the attenuation for all temperatures increases with increasing frequency, the attenuation for constant frequencies, is observed to be a nonmonotonic function of the anneal temperature (Fig. 2). Below 800 K the attenuation (for fixed frequency) remains constant. The attenuation increases rapidly with temperature from 800 to 900 K. Although the attenuation continues to increase between 900 and 975 K it is at a much slower rate. Above 975 K the attenuation again rapidly rises with temperature. Figure 2 also demonstrates that the magnitude of the variation in attenuation over the entire anneal temperature range is more pronounced at higher frequencies.

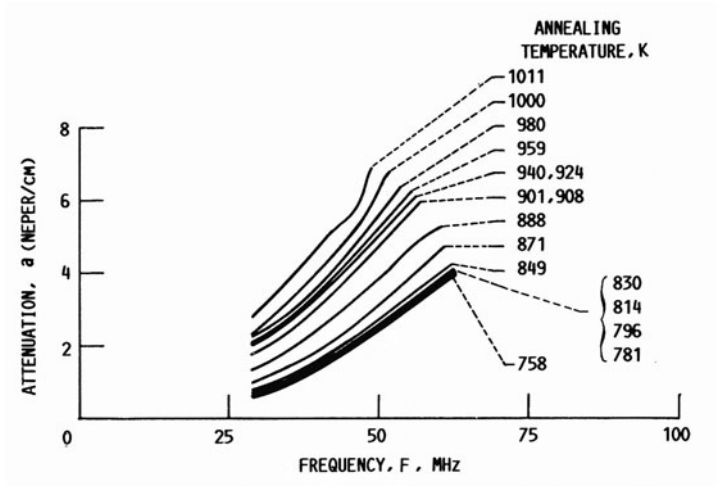


Figure 1. Ultrasonic attenuation as a function of frequency.

Figure 2.
Ultrasonic attenuation as a function of anneal temperature (solid curves). The dash curve is the full width at half maximum of the (200) x-ray diffraction peak.

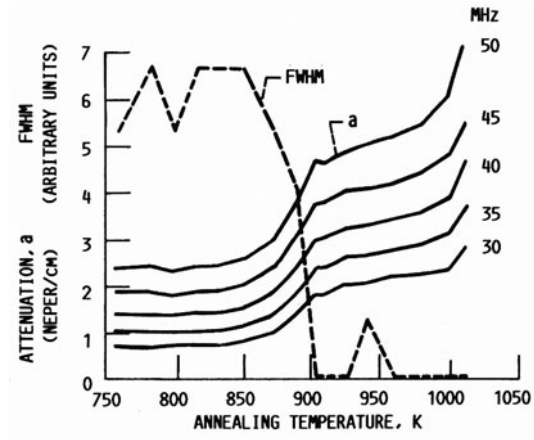


## X-Ray Analysis

The full width at half maximum (FWHM) of the (200) x-ray Bragg peak varies considerably over the annealing temperature range (Fig. 2). For temperatures below 850 K the FWHM remains relatively constant. The FWHM rapidly decreases over the range 850 to 900 K. This is an indication of increasing crystalline order with increasing anneal temperature. Temperatures above 901 K resulted in a relatively constant FWHM. The uncertainty in this measurement is relatively large as evidenced by the fluctuating FWHM at both low and high anneal temperatures.

## Metallographic Results

Typical photomicrographs for the face and edge sides are shown in Figs. 3 to 8 for anneal temperatures of 758, 814, 871, 901, 940, and 1011 K (labeled $T_1$-$T_6$), respectively. As the two perpendicular edges exhibited similar microstructure, only data for one edge is shown.

Photomicrographs of the face plane illustrate little change with annealing temperature until it equaled approximately 901 K where the unclear, worked structure remaining after lower temperature heat treatments (Figs. 3(c), 4(c), and 5(c)) is replaced by a normal grain struc-

ture (Fig. 6(c)). Higher annealing temperatures (Figs. 7(c) and 8(c)) result in little additional change except for grain growth. While examination of the face sections reveals a sharp transition in microstructure at 901 K, the edge planes show a much more gradual effect. As the annealing temperature is increased above 871 K the elongated grain structure visible in Figs. 3(b) and 4(b) is slowly replaced by a normal grain configuration (Figs. 5(b) and 6(b)) until recrystallization is nearly complete (Fig. 7(b)) and grain growth occurs (Fig. 8(b)).

Transmission Electron Microscopy

Transmission electron photomicrographs for six anneal temperatures are also shown in Figs. 3 to 8. Below 800 K TEM found only localized areas with high and low dislocation densities (Fig. 3(a)). The high and low density regions are dark and light areas, respectively, in Fig. 3. At 814 K, nucleated crystallites have started to form (Fig. 4(a)) with the nucleated crystallites varying in size and exhibiting boundaries constructed of an intertwined collection of dislocations. Figure 4 also contains regions that appear to be just forming into crystallites; these regions are believed to be germ nuclei that have just transformed into nucleation sites. At 871 K fully developed crystallites with planar boundaries co-exist with localized regions of low and high dislocation densities (Fig. 5(a)). The 901 K anneal exhibits larger crystallites having both narrow step-like boundaries and boundaries containing a collection of oriented dislocation pile-ups (Fig. 6(a)); additionally, isolated and interconnected dislocations are present within the crystallites. After a 940 K anneal (Fig. 7(a)) the boundaries tend to have a collection of dislocations randomly attached to them, and both isolated and interconnected dislocations are present within the crystallites. At the highest anneal temperature, 1011 K, (Fig. 8(a)), only random isolated dislocations are present within the crystallites.

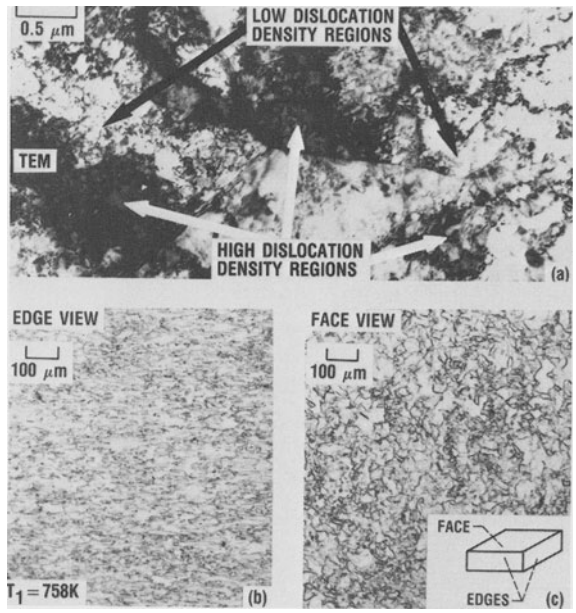


Figure 3. Transmission electron micrograph, and edge and side metallographic views of sample annealed at 758 K ($T_1$).

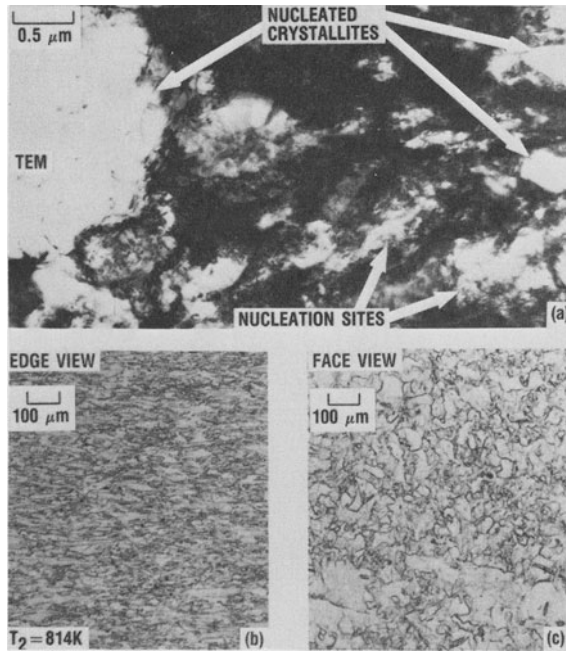


Figure 4. Transmission electron micrograph, and edge and side metallographic views of sample annealed at 814 K ($T_2$).

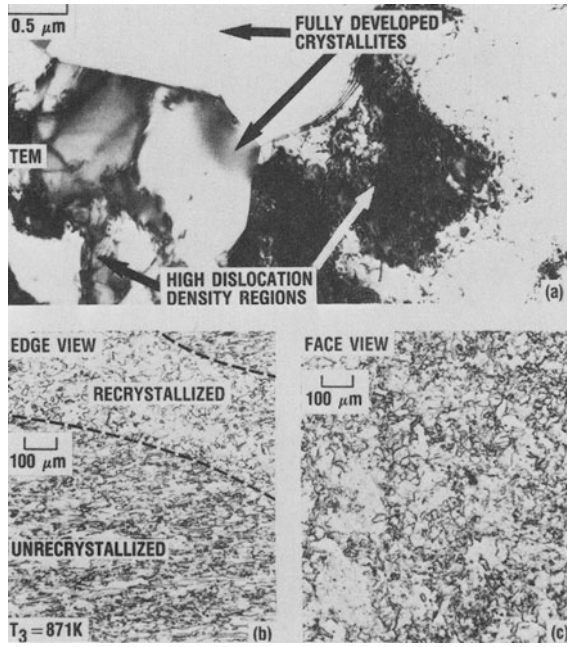


Figure 5. Transmission electron micrograph, and edge and side metallographic views of sample annealed at 871 K ($T_3$).

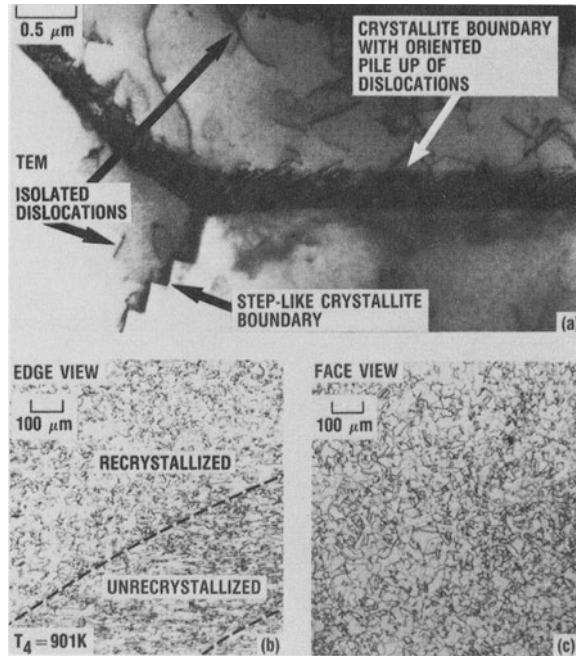


Figure 6. Transmission electron micrograph, and edge and side metallographic views of sample annealed at 901 K ($T_4$).

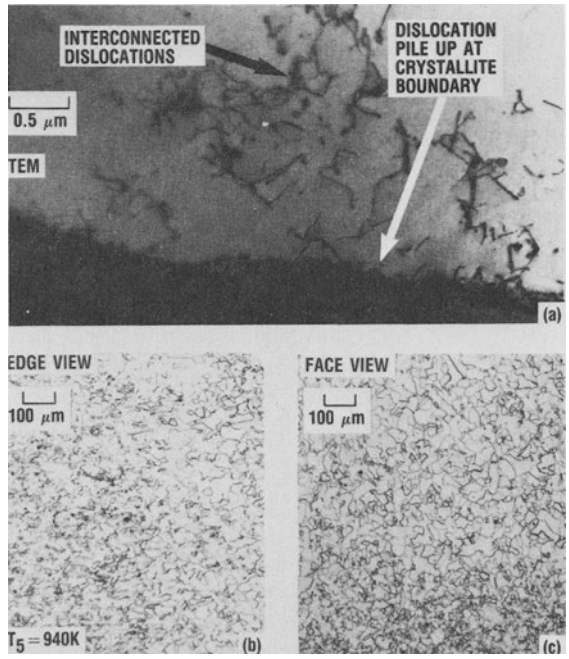


Figure 7. Transmission electron micrograph, and edge and side metallographic views of sample annealed at 940 K ($T_5$).

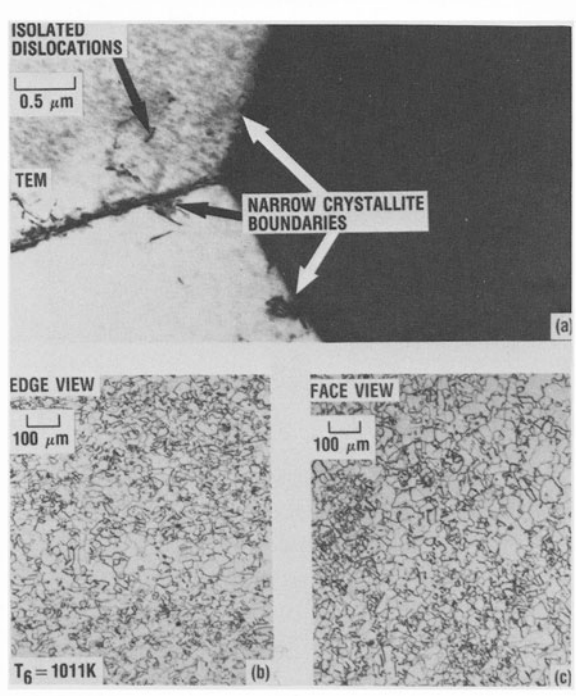


Figure 8. Transmission electron micrograph, and edge and side metallographic views of sample annealed at 1011 K ($T_6$).

Correlation Between Ultrasonic Attenuation and Thermal Kinetics

Figure 9 shows the value of the key variable N (dashed-dotted curve) determined by fitting the data shown in Fig. 1 to

$$a = CF^N. \tag{4}$$

The percent of recrystallization $V_R/V$ determined by use of Eq. (3) is shown as a solid curve. Here $S = 4\pi/3$, $G = 3$ μm/hr, $U = 80$ Kcal/mole[3,8-10] and the free parameter $N_0$ is taken to be $2 \times 10^{18}$ germ nuclei/cm$^3$. Also shown is the percent of recrystallization, obtained from the photomicrographs,[9] for samples exhibiting about 25 to 75 percent recrystallization; larger and smaller percents could not be precisely determined by optical methods.

## DISCUSSION

During the entire annealing process the attenuation at a fixed frequency either remains constant or increases with increasing anneal temperature. The dislocation density is not known quantitatively, it does, however, decrease from an extremely large to a low value as recovery and recrystallization takes place over the anneal temperature range. Therefore, dislocation damping cannot be the dominant attenuation mechanism causing the large change in attenuation observed during recrystallization. From this result it will be assumed that the grain boundary scattering is the dominant attenuation mechanism during the recrystallization process.

The onset of recrystallization is identified as the temperature at which the first germ nuclei transform into nucleated crystallites. Acoustically the onset of recrystallization begins in the temperature

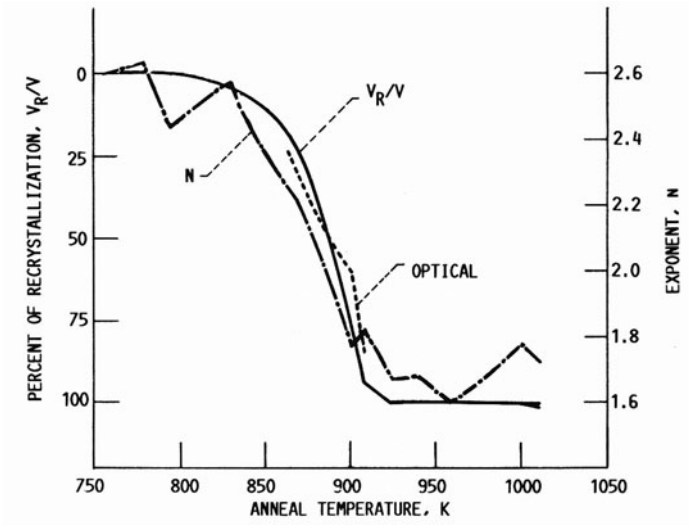


Figure 9. Recrystallization percent $V_R/V$ determined by use of equation (3) (solid curve), light optical metallographic techniques (dotted curve) and calculated exponent N (dash-dotted curve) as a function of annealing temperature.

range 796 to 814 K where the attenuation first starts to increase (light shaded region in Fig. 10). At these anneal temperatures the small nucleated crystallites are acoustically Rayleigh scatterers yielding the large value of the exponent N (Fig. 9).

Increasing the anneal temperature produces an increasing number of nucleated crystallites and simultaneously enhances the growth rate of previously nucleated crystallites. Therefore, above 814 K there is a mixed system of Rayleigh (newly formed crystallites) and nearly stochastic (growing crystallites) scatterers. For temperatures between 814 and 975 K, the magnitude of the attenuation is expected to increase while the exponent N should decrease (see Eq. (1)). This is in agreement with Figs. 2 and 9 and is identified as the recrystallization temperature range in Fig. 10 (dark shaded region).

The completion of recrystallization is identified as the temperature at which all the germ nuclei are depleted. That is, the germ nuclei have either transformed into nucleated crystallites or have been swallowed up by growing crystallites. The completion of recrystallization occurs between 960 and 975 K and is shown in Fig. 10 as a light shaded region.

Above 975 K pure grain growth is observed (cross-hatched region in Fig. 10). Since the grains are relatively large (approximately 50 μm diameter), for temperatures above 975 K, they (growing at rate of about 3 μm/hr) are stochastic scatterers; thus the attenuation above 975 K should increase while the exponent N should remain a constant (Eq. (1)) in agreement with Figs. 2 and 9. It should be noted here, that the attenuation in the pure grain growth region has been investigated previously[13] and found to scale with the ratio of mean grain diameter to sound wavelength indicating that dominant attenuation mechanism is grain boundary scattering.

Both the recrystallized function $V_R/V$ and the exponent N possess similar temperature dependence (Fig. 9). The thermal kinetic results supports the attenuation data and is understood as follows. The probability of a germ nuclei transforming into a nucleated crystallite increases with increasing anneal temperature. Therefore, an initially

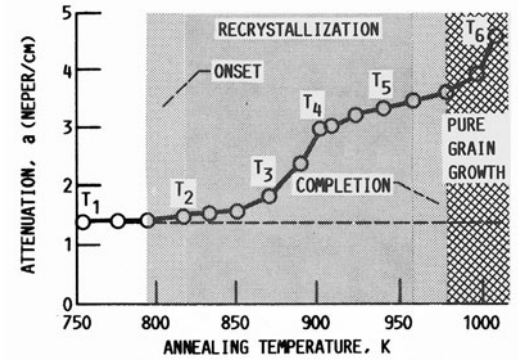


Figure 10. Attenuation as a function of annealing temperature at 40 MHz. The light shading in the figure indicates acoustic identification of the temperature ranges for onset and completion of recrystallization. The dark shading indicates the recrystallization temperature range. The cross-hatched region indicates the onset of pure grain growth. The temperature labels $T_1$ and $T_6$ refer to the data shown in Figs. 3 to 8 respectively.

slow recrystallization rate is followed by a rapid increase in the rate. Also, the germ nuclei transform simultaneously with the growth of previous nucleated crystallites. These growing crystallites tend to swallow up other germ nuclei so that the density of germ nuclei decreases. Therefore, there are two mechanisms that lead to a decrease in germ nuclei density. The germ nuclei become activated and transform into crystallites or they get swallowed up by growing crystallites. As a result the recrystallization rate (or the rate of formation of Rayleigh scatters) at high temperatures decreases.

The FWHM of the diffraction peak obtains a minimum value at 901 K. This is an indication that the highest crystalline order has been obtained. However, the edge photomicrographs clearly indicate that recrystallization is incomplete (Fig. 6(b)). Bragg backscattered x-rays probe only a few microns, so that, the FWHM diffraction data indicates that the surface of the sample has recrystallized at 901 K. This is optically supported by comparing Fig. 5(b) and (c) with Fig. 6(b) and (c).

## CONCLUSION

Ultrasonic attenuation was measured for cold worked Nickel 200 samples annealed at increasing temperatures. Localized dislocation density variations, crystalline order, and volume percent of recrystallized phase were examined over the annealing temperature range using transmission electron microscopy, x-ray diffraction, and metallography. The exponent of the frequency dependence of the attenuation has been found to be a key variable relating ultrasonic attenuation to the thermal kinetics of the recrystallization process. Measurement of this key variable allows for the ultrasonic determination of onset, degree, and completion of recrystallization.

X-ray, metallography, and TEM analysis individually cannot characterize the state of the recrystallization process. However, the ultrasonic attenuation, being extremely sensitive to the formation of small scatterers and having a wide dynamic range to large scatters, is able to characterize the recrystallization process.

REFERENCES


1. R.E. Reed-Hill, "Physical Metallurgy Principles," 2nd ed., Van Nostrand, New York, 1973.

2. G.E. Dieter, "Mechanical Metallurgy," McGraw-Hill, New York, 1961.

3. L.M. Clarebrough, M.E. Hargreaves, and G.W. West, Proceedings of the Royal Society, Part A, 232, 252-270 (1955).

4. J.F. Nicholas, Philosophical Magazine, 46, 87-97 (1955).

5. R. Truell, C. Elbaum, and B.B. Chick, "Ultrasonic Methods in Solid State Physics," Academic Press, NY, 1969.

6. E.P. Papadakis, Journal of the Acoustical Society of America, 37, 711-717 (1965).

7. A. Granato and K. Lucke, Journal of Applied Physics, 27, 583-593 (1956).

8. M. Avrami, Journal of Chemical Physics, 7, 1103-1112 (1939).

9. M. Avrami, Journal of Chemical Physics, 8, 212-224 (1940).

10. M. Avrami, Journal of Chemical Physics, 9, 177-184 (1941).

11. E.R. Generazio, Materials Evaluation, 43, 995-1004 (1985).

12. P. Gay, P.B. Hirsch, and A. Kelly, Acta Metallurgica, 1, 315-319 (1953).

13. E.R. Generazio, Materials Evaluation, 44, 198-202, 208 (1986).